Check for updates

Water Supply

IWA PUBLISHING

© 2022 The Authors

Water Supply Vol 22 No 5, 4852 doi: 10.2166/ws.2022.156

Gallic acid enhanced bisphenol A degradation through Fe^{3+}/peroxymonosulfate process

Lei Zhang[a], Zheng Qian[a], Lingzhen Wang[a], Pengkang Jin[a,b] and Shengjiong Yang[a,*]

[a] Key Laboratory of Environmental Engineering, Xi'an University of Architecture and Technology, No.13, Yanta Road, Xi'an, Shaanxi 710055, China
[b] School of Human Settlements and Civil Engineering, Xi'an Jiaotong University, Xi'an, Shaanxi Province 710049, China
*Corresponding author. E-mail: yangshengjiong@163.com, yangshengjiong@xauat.edu.cn

SY, 0000-0002-0730-5873

ABSTRACT

Fe^{2+} is widely used for effective peroxymonosulfate (PMS) activation to eliminate refractory organics. However, Fe^{2+}/PMS process suffers from difficulty on Fe^{2+} regeneration. Herein, we report an Fe^{3+}/PMS process by using gallic acid (GA) as an effective promotor for efficient degradation of bisphenol A (BPA). The process exhibited considerable oxidation performance in the pH range of 3.0–10.0. Higher concentration of Fe^{3+}/GA complex exhibited better BPA degradation performance whereby BPA could be completely degraded within 4 mins. Reactive oxidation species (ROS) quenching experiments, electron paramagnetic resonance (EPR) analysis, and methyl phenyl sulfoxide (PMSO) probing experiments revealed that sulfate radical ($SO_4^{\bullet-}$), hydroxyl radical ($HO^{\bullet}$), and ferryl species are involved and responsible for the BPA degradation. Electrochemical analysis and density function theory (DFT) calculation explored that the self-oxidation of GA boosted the reduction of Fe^{3+} into Fe^{2+} for continuous activation of PMS. The GA boosted Fe^{3+}/PMS system reached an intriguing mineralization efficiency of 86.4%. Findings from this work proposed references to improve the oxidation performance of Fenton-like reaction and provided new sight into the Fe^{3+}/Fe^{2+} cycling.

Key words: activation, degradation, Fe^{2+}, ferryl species, peroxymonosulfate

HIGHLIGHTS

- Gallic acid significantly promoted the Fe^{3+}/Fe^{2+} cycling.
- The oxidation performance of Fe^{3+}/peroxymonosulfate could be largely elevated by gallic acid.
- More than 86.4% of BPA could be mineralized by the Fe^{3+}/peroxymonosulfate/gallic acid process.

GRAPHICAL ABSTRACT

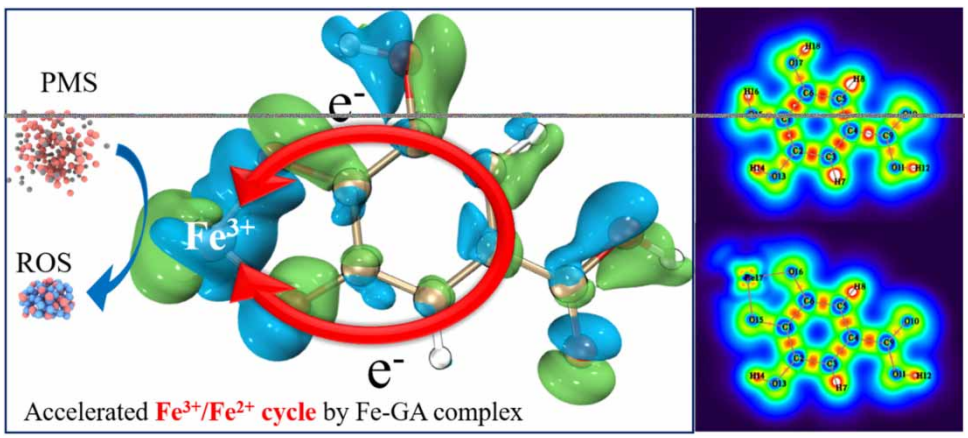

This is an Open Access article distributed under the terms of the Creative Commons Attribution Licence (CC BY 4.0), which permits copying, adaptation and redistribution, provided the original work is properly cited (http://creativecommons.org/licenses/by/4.0/).

Downloaded from http://iwaponline.com/ws/article-pdf/22/5/4852/1076437/ws022054852.pdf
by guest

1. INTRODUCTION

Persulfate, including peroxymonosulfate (PMS) and peroxydisulfate (PDS), have acquired increasing attention in eliminating refractory organic pollutants. Persulfate can be activated by heat (Milh *et al.* 2021), radiation (Wang *et al.* 2021a), and transition metals (Gao *et al.* 2021), among others. Various reactive oxidation species (ROS) including sulfate radical, hydroxyl radical, singlet oxygen, etc., can be generated during persulfate activation, rendering the degradation of coexisting organic pollutant. Amongst the activation processes, transition metal (ions or oxides) is the most convenient method for PMS and PDS activation (Wang *et al.* 2021b). Co is exemplified in many works undertaken by the most effective catalysts for PMS activation (Huang *et al.* 2022). Another example of what is meant is that Ag exhibited the best catalytic performance for PDS activation (King 1928). However, the wide use of Ag and Co cannot be considered due to the high price of Ag and the toxicity of Co, respectively. Although cobalt ferrite based heterogeneous PMS activation could largely minimize the secondary pollution of Co, the pollutant degradation efficiency became the primary consideration due to the limited mass-transfer between solid catalyst and solution (Qiu *et al.* 2021). Therefore, homogeneous activation of PMS by Fe is an optimum selection because of the low cost and non-toxicity of Fe salt.

Fe^{2+} is well known as a unique catalyst in Fenton reaction for hydrogen peroxide activation, it also has been reported that the PMS and PDS can be activated by Fe^{2+} solution with a similar mechanism (Wang *et al.* 2020a). However, the use of Fe^{2+} still suffers from several vital problems. To begin with, the regeneration of Fe^{2+} from Fe^{3+} is comparatively difficult (Wang *et al.* 2020a), rendering decreased PMS activation performance. More importantly, Fe^{3+} generated after PMS activation always tended to hydrolysis and is likely to form cationic polynuclear hydrolysis products with large size, like $Fe(OH)_3$ (Ristić *et al.* 2006). The hydrolysis product of Fe^{3+} would serve as coagulant and slightly enhance the pollutant removal efficiency (Shen *et al.* 2014). However, the Fe species would be then totally deactivated. To solve this problem, strong reductants, such as hydroxylamine (Li *et al.* 2022), MoS_2 (Song *et al.* 2020), boron (Sirés *et al.* 2007), etc., were trialed in the reaction system. The addition of reductant could regenerate Fe^{2+} via the efficient reduction of Fe^{3+}, which prevented the hydrolysis of Fe^{3+} and boosted the PMS activation performance at meantime. However, the addition of reductant is always expensive. To prevent the hydrolysis of Fe cations, the use of chelating agents is also an alternative method. It is well known that ethylenediaminetetraacetic acid (EDTA) and nitrilotriacetic acid (NTA) could effectively chelate with Fe ions and maintain Fe ion in soluble forms with Fe-chelate complex (Zhou *et al.* 2008; Zhang *et al.* 2016). Furthermore, the chelate agent usually possesses strong electron donation performance, which would facilitate the Fe^{3+}/Fe^{2+} cycling during the Fenton reaction for better pollutant degradation efficiency. However, the chelate agents are always high cost. More suitable chelate agents should be used.

Natural polyphenols extracted from plant is full of benzenic hydroxyl groups and strong electron-donating capacity, where tannins is the most typical one (Wang *et al.* 2021c). It has been reported that tannins can coordinate with various metal ions for the synthesis of metal-polyphenol coordination particles (Wei *et al.* 2016; Wang *et al.* 2020b). Inspired by this, it can be can be expected that tannins-metal complex might be useful in a Fenton-like process to prevent Fe^{3+} hydrolysis and facilitate Fe^{3+}/Fe^{2+} cycling. In this study, gallic acid (GA), the monomer of tannins, was used to create an Fe^{3+}/GA complex solution to effectively activate PMS. Bisphenol A (BPA) is used as the representative pollutant to systematically evaluate the oxidation performance of the Fe^{3+}/GA/PMS system. The influences of various reaction conditions, mechanism, and ROS evolution are carefully investigated. In addition, the BPA degradation performance in various coexisting chemicals was also evaluated as an example of potential application.

2. MATERIAL AND METHODS

2.1. Chemical reagents

Chemicals used in this study were at least analytical grade and directly used without further purification. Peroxymonosulfate triple salt ($2KHSO_5{\cdot}KHSO_4{\cdot}K_2SO_4$) was used as PMS source, which was purchased from Macklin Biochemical Co., Ltd (Shanghai, China). Spin-trapping reagent, including 5,5-Dimethyl-1-pyrroline N-oxide (DMPO) and 2,2,6,6-Tetramethyl-4-piperidinol (TEMP), and probe reagent, including methyl phenyl sulfoxide (PMSO, C_7H_8OS, 98%) and methyl phenyl sulfone ($PMSO_2$, $C_7H_8O_2S$, 98%), were purchased from Macklin Biochemical Co., Ltd (Shanghai, China). HNO_3, $Fe(NO_3)_3{\cdot}9H_2O$, NaCl, Na_2SO_4, KH_2PO_4, $NaHCO_3$ were all obtained from Kermel Chemical Reagent Co., Ltd (Tianjin, China). Chromatographic grade acetonitrile and methanol were purchased from Thermo Fisher. Bisphenol A (BPA) was purchased from Aladdin Biochemical Technology Co., Ltd (Shanghai, China). Deionized (DI) water (18 mΩ) was used throughout the study.

Downloaded from http://iwaponline.com/ws/article-pdf/22/5/4852/1076437/ws022054852.pdf
by guest

2.2. BPA degradation test

All the catalytic BPA degradation experiments were conducted in 120 mL vessels at 25 ± 1 °C controlled with a water bath. Typically, a certain amount of Fe^{3+} stock solution and GA solution was added in BPA-containing DI water with a pre-adjusted pH value. Then, certain volumes of PMS stock solution was added into the mixture to initiate the BPA degradation process. At a given time interval, 1 mL solution sample was collected. The samples were immediately filtered by 0.22 μm membrane, and mixed with 0.5 mL methanol to terminate the reaction.

2.3. Analytical methods

The BPA concentration of all samples was measured with a high-performance liquid chromatography (HPLC, Shimazu, 20A, Japan). The mobile phase was composed of acetonitrile (40%) and water (60%) with a flow rate of 1 mL min^{-1}. The wavelength was set at 278 nm, a C18 HC column (4.6 μm) was used for the separation of BPA and other organic compounds. All experiments were conducted in triplicate and were measured within 10 min after reaction. Attenuated total internal reflectance Fourier transform infrared spectroscopy (ATR-FTIR, Nicolet iS50, Thermo Scientific, USA) with Thermo Scientific OMNIC software were used for the investigation of functional groups of the Fe/GA complex. The concentration of Fe^{2+} was monitored on a UV-Vis Spectrophotometer (T6 General) with 1,10-Phenanthroline spectrophotometric method (Chemical products for industrial use: ISO 6685-1982). Total organic carbon (TOC) values were determined by a total organic carbon analyzer (TOC-V CPH). All electrochemical measurements were performed on an Electrochemical Workstation (CHI660E) with a three-electrode system (Miao *et al.* 2020), where Ag/AgCl electrodes were used as reference electrode, Pt wire electrode as the counter electrode, and glassy carbon electrode as the working electrode.

The electron structure of GA and Fe/GA complex was investigated by Gaussian 16 W.1B quantum chemical software (Gaussian 16, Revision C.01 2019). B3LYP method was used in the basis set of 6-31G (d) for C, H, O atoms, and Lanl2dz for Fe atoms with a long-range correction of density functional theory (DFT-D3). All the atoms were free to move in the optimization process. Fukui index calculation and localized orbital locator (LOL) analysis was conducted by the Multiwfn software package (Lu & Chen 2012).

3. RESULTS AND DISCUSSION

3.1. Apparent BPA degradation

The BPA degradation by various Fe/PMS systems was firstly evaluated, which can be seen in Figure 1. It is found that BPA could not be degraded by PMS solution without the addition of Fe species, less than 3% of BPA was degraded by PMS solution. Not surprisingly, the simultaneous addition of Fe^{2+} and PMS could effectively degrade BPA, and about 60.2% of BPA was degraded within 10 minutes. It can be seen that the BPA degradation by Fe^{2+}/PMS obviously consisted of two stages. In the preliminary 2 min, more than 58.5% of BPA was degraded, and then slightly increased to 60.2% with very

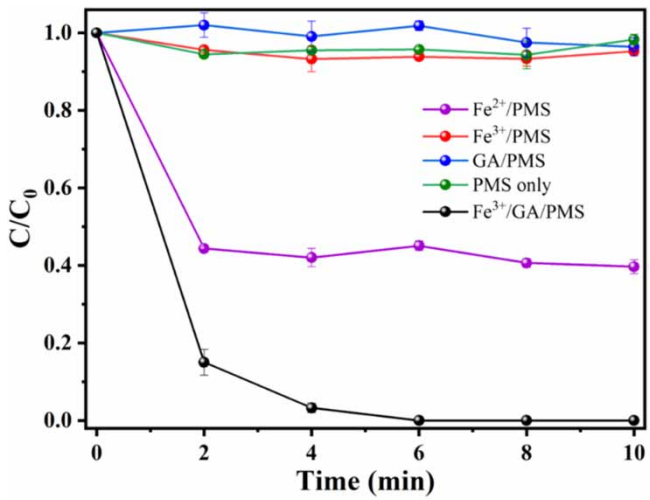

Figure 1 | BPA degradation by different Fenton-like system. (Experimental conditions: [Fe^{2+}] = 100 μM, [Fe^{3+}] = 100 μM, [GA] = 100 μM, [PMS] = 1 mM, [BPA] = 40 μM, [pH_0] = 5.0 ± 0.1, [Temperature] = 25 ± 0.2 °C).

Downloaded from http://iwaponline.com/ws/article-pdf/22/5/4852/1076437/ws022054852.pdf
by guest

slow reaction rate until the reaction was terminated. This phenomenon manifested that: (1) Fe^{2+} could effectively activate PMS and (2) Fe^{3+}/Fe^{2+} cycle in PMS solution is rather difficult. This deduction further proved that same concentration of Fe^{3+} exhibited negligible PMS activation performance, about 3% of BPA was degraded by Fe^{3+}/PMS (almost the same with PMS solution). However, the BPA degradation efficiency was considerably elevated when GA was added in the Fe^{3+}/PMS system. Figure 1 shows that BPA could be completely degraded within 6 mins with a kinetic rate k of 0.85 min^{-1} obtained from a pseudo-first order kinetic model (Text S1). This observation evidenced strong promotion effect of GA toward Fe^{3+}/PMS. Considering the rate-limiting by Fe^{3+}/Fe^{2+} process, the addition of GA might be likely to continuously reduce Fe^{3+} into Fe^{2+}, therefore facilitating the PMS activation performance. This process reminded that GA is capable of reduction as electron donator, therefore, the PMS activation performance by GA was also confirmed. As shown, PMS could not be activated by GA in the absence of Fe^{3+}, indicating that GA could not directly transfer electrons to PMS. It also reminded that PMS was activated by the Fe-GA complex.

3.2. The effect of various reaction conditions

The effect of initial pH (pH_0) on the BPA degradation by Fe^{3+}/GA/PMS process was firstly investigated. As shown in Figure 2(a), about 95% of BPA could be degraded at pH_0 3.0 within 10 min. It can be seen that increased pH_0 positively

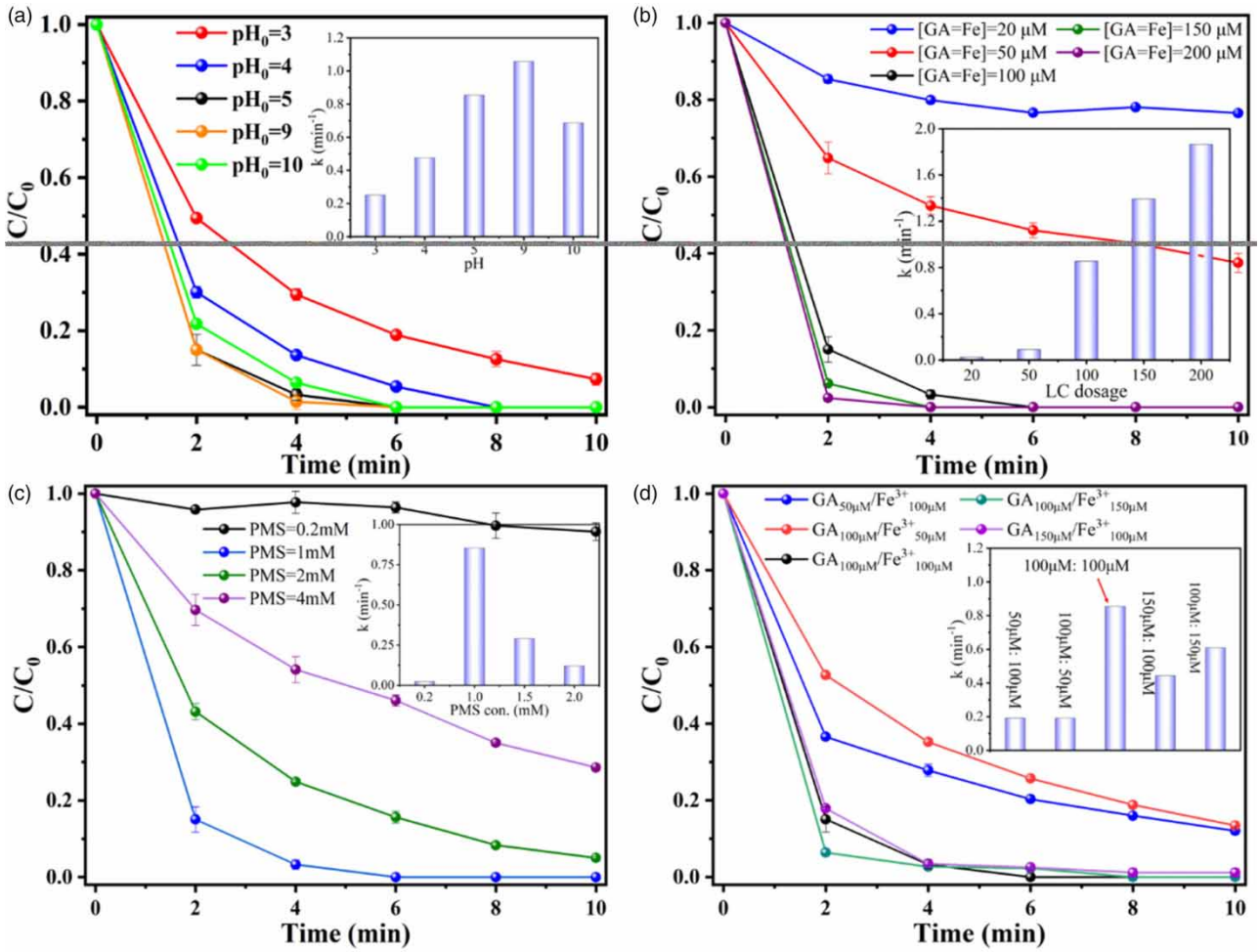

Figure 2 | Effect of various reaction condition, (a) effect of initial solution pH ($[Fe^{3+}] = 100$ μM, [GA] = 100 μM, [PMS] = 1 mM, [BPA] = 40 μM, $[pH_0] = 3.0, 4.0, 5.0, 9.0, 10.0 \pm 0.1$, [Temperature] = 25 ± 0.2 °C), (b) effect of LC dosage ($[Fe^{3+}]$ = [GA] = 20, 50, 100, 150, 200 μM, [PMS] = 1 mM, [BPA] = 40 μM, $[pH_0] = 5.0 \pm 0.1$, [Temperature] = 25 ± 0.2 °C, (c) effect of PMS concentration ($[Fe^{3+}] = 100$ μM, [GA] = 100 μM, [PMS] = 0.2, 1, 2, 4 mM, [BPA] = 40 μM, $[pH_0] = 5.0 \pm 0.1$, [Temperature] = 25 ± 0.2 °C), and (d) effect of Fe^{3+}/GA molar ratio ($[Fe^{3+}]$ = 50, 100, 150 μM, [GA] = 50, 100, 150 μM, [PMS] = 1 mM, [BPA] = 40 μM, $[pH_0] = 5.0 \pm 0.1$, [Temperature] = 25 ± 0.2 °C); all the inset figures exhibit reaction rate k of corresponding conditions.

Downloaded from http://iwaponline.com/ws/article-pdf/22/5/4852/1076437/ws022054852.pdf
by guest

influenced the BPA degradation when $pH_0 \leq 9$. However, when pH_0 increased to 10, the BPA degradation was slightly inhibited. The *pKa* of PMS is 9.4 (Guan *et al.* 2011), it usually exists in the formation of H_2SO_5 at stronger acidic conditions, which is comparatively stable and more difficulty to be activated. On the contrary, it also has been reported that PMS could be activated by base, rendering better BPA degradation at higher solution pH (Qiu *et al.* 2019). However, strong alkaline conditions might cause the self-quenching of excessive reactive oxidation species, explaining the slightly inhibited BPA degradation when $pH_0 \geq 10$. In addition, the BPA degradation also correlated with the self-oxidation of GA, which is discussed in section 3.4.

The mixture of Fe^{3+} and GA was defined as a liquid catalyst (LC) for PMS activation, the effect of different LC concentration was evaluated. As shown in Figure 2(b), when the concentration of $[Fe^{3+}] = [GA] = 20$ uM, only 23.5% of BPA was degraded. With the increased LC concentration, the BPA degradation performance increased accordingly. When the concentration of $[Fe^{3+}] = [GA] = 200$ uM, BPA could be dramatically degraded within 4 min. It can be easily explained that the increased LC dosage could supply more active catalytic species, rendering the significantly increased PMS activation and BPA degradation. It can be further proved that the correlation between k and LC concentration highly fitted with a linear correlation of $k = 0.011[con.(Fe^{3+} = GA)] - 0.2909$ (Figure S1).

The effect of PMS concentration was also evaluated, which is shown in Figure 2(c). When the PMS concentration was 0.2 mM, only 10% of BPA could be degraded. Further increased PMS concentration could effectively elevate the BPA degradation under the same concentration of liquid catalysts. It seems that the BPA degradation is positively correlated with the concentration of coexisting PMS. However, when the PMS concentration was higher than 1 mM, the performance of BPA degradation was significantly inhibited, which is reminiscent of $SO_4^{\bullet-}$ and $HO^{\bullet}$ scavenging by excessive PMS. Similar results have been reported elsewhere (Wang *et al.* 2021d; Ouyang *et al.* 2022). This result indicated that free radicals were effectively generated and dominated for BPA degradation.

Figure 2(d) shows the BPA degradation performance of Fe^{3+}/GA/PMS system under different molar ratio of Fe^{3+}:GA. When the concentration of GA was 100 uM, the BPA degradation efficiency positively correlated with increased Fe^{3+} ions. On the other hand, when the concentration of Fe^{3+} was fixed at 100 uM, the increased GA concentration also exhibited a positive effect. However, 150 uM of GA exhibited an inhibition effect. It can be explained that excessive GA would quench more generated ROS, rendering decreased BPA degradation. Overall, Fe^{3+}:GA = 1:1 is the optimum condition for effective PMS activation.

3.3. Identification of reactive oxidation species

EPR analysis was firstly used for the identification of generated ROS during the PMS activation process by using 5,5-dimethyl-l-pyrrolidine N-oxide (DMPO) as spin trapping reagent (Chen *et al.* 2021). Very slight signal with intensity of 1:2:2:1 could be observed in PMS solution, which is widely known as the signal of DMPO-OH. In the Fe^{3+}/GA system, a series overlapped signal of DMPO-OOH (Meng *et al.* 2021), DMPO-OH, and DMPO-SO_4 could be observed. It also can be seen that the intensity decreased with the reaction time. Therefore, it can be deduced that $HO^{\bullet}$ and $SO_4^{\bullet-}$ were generated during the PMS activation by the Fe^{3+}/GA system. In addition, the existence of $O_2^{\bullet-}$ in the Fe^{3+}/GA/PMS system was also investigated in methanol solution. The results clearly showed the signal of $O_2^{\bullet-}$, and the intensity also decreased with reaction time. Moreover, 2,2,6,6-tetramethylpiperidine (TEMP) was used for the identification of singlet oxygen ($^1O_2$). It can be seen that the signal of $^1O_2$ (triplet pattern) could be observed with significant intensity, indicating the widely generated $^1O_2$ during the PMS activation process (Yang *et al.* 2021a). However, a stronger signal intensity of $^1O_2$ could be found in PMS solution. Therefore, the contribution of $^1O_2$ for BPA degradation is still debatable.

To further confirm the involvement of reactive oxidation species, the scavenging experiment was further conducted. As known, methanol was commonly used as an effective scavenger for both $SO_4^{\bullet-}$ ($k = 1.6 - 7.7 \times 10^7\ M^{-1}\ s^{-1}$) and $HO^{\bullet}$ ($k = 1.2 - 2.8 \times 10^9\ M^{-1}\ s^{-1}$), and tert-butanol (TBA) was usually used as the scavenger for $HO^{\bullet}$ because of its higher reactivity with $HO^{\bullet}$ ($k = 3.8 - 7.6 \times 10^8\ M^{-1}\ s^{-1}$) (Li *et al.* 2017). As can be seen in Figure 3(d), the addition of TBA (25 mM) negatively affected the oxidation performance of Fe^{3+}/GA/PMS system that the BPA degradation efficiency decreased to 62.4% when comparing with 100% in the abscence of TBA. This result manifested that $HO^{\bullet}$ was involved. Moreover, the coexistence of methanol exhibited more serious inhibition on BPA degradation than TBA where only 4.1% of BPA was degraded. The completely terminated reaction indicated the significantly generated $SO_4^{\bullet-}$ during the PMS activation process. Therefore, the generation of $SO_4^{\bullet-}$ and $HO^{\bullet}$ can be confirmed in the Fe^{3+}/GA/PMS system. In addition, p-BQ was further added into the Fe^{3+}/GA/PMS system to evaluate the role of $O_2^{\bullet-}$ because p-BQ could effectively react with $O_2^{\bullet-}$. As shown in Figure 3(a),

Downloaded from http://iwaponline.com/ws/article-pdf/22/5/4852/1076437/ws022054852.pdf
by guest

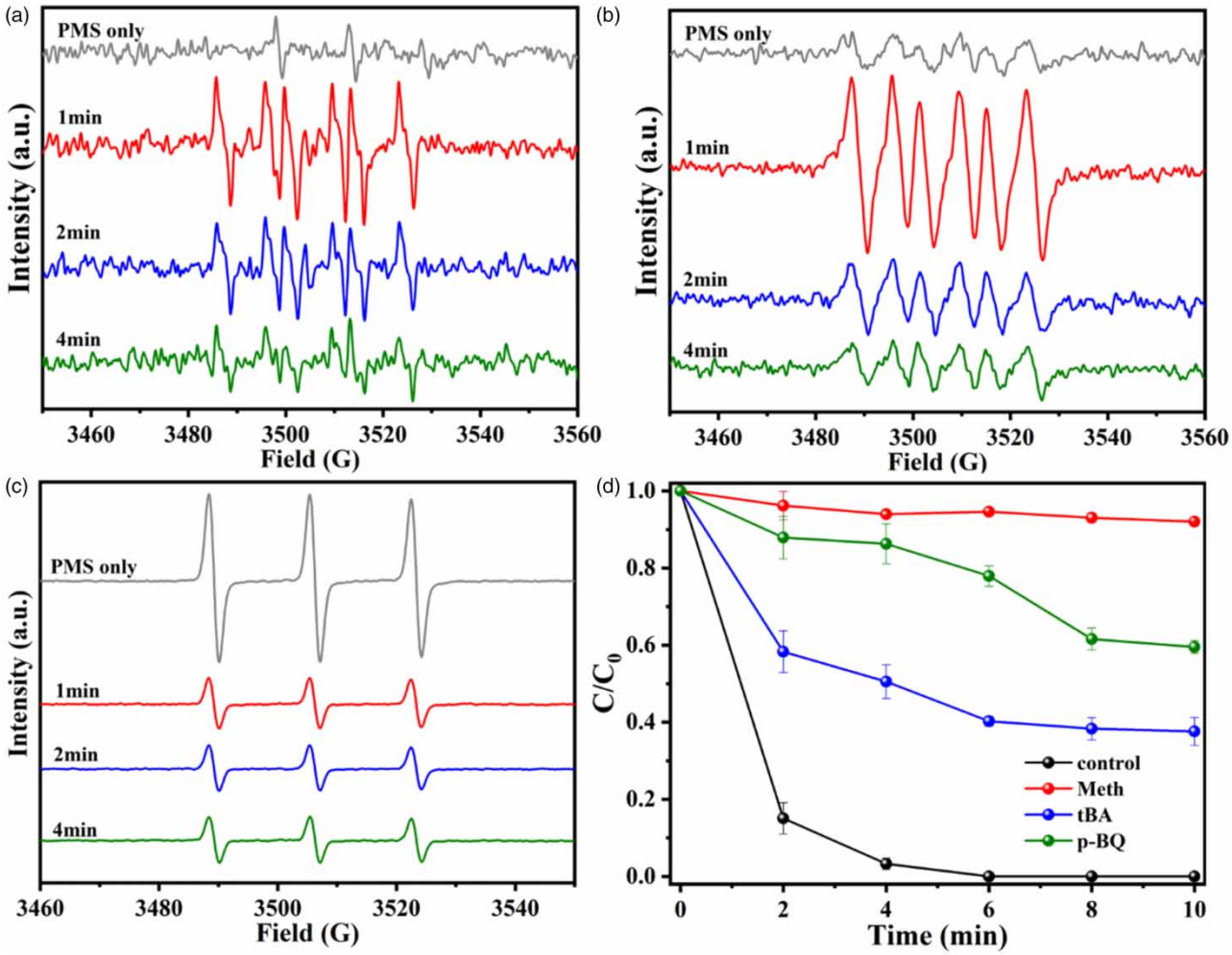

Figure 3 | EPR analysis by: (a) DMPO in water, (b) DMPO in methanol, (c) TEMP in water, and (d) scavenging experiments ($[Fe^{3+}] = 100$ μM, [GA] = 100 μM, [PMS] = 1 mM, [BPA] = 40 μM, [Meth] = 500 mM, [TBA] = 500 mM, [p-BQ] = 20 mM, [pH_0] = 5.0 ± 0.1, [Temperature] = 25 ± 0.2 °C).

the existence of p-BQ significantly decreased the BPA degradation, indicating that $O_2^{\cdot-}$ also participated in the BPA degradation process. This result agreed well with results obtained from EPR analysis that DMPO-OOH and DMPO-O_2 adduct were generated in this process.

More importantly, it has been reported that aqueous ferryl species (Fe(IV)) was involved during the PMS and PDS activation by using Fe^{2+}/Fe^0 as catalysts (Wang *et al.* 2020c). Considering the possible Fe^{3+}/Fe^{2+} cycle caused by GA, Fe(IV) might be also generated in the process for BPA degradation. To confirm the generation of Fe(IV) species in the Fe^{3+}/GA/PMS system, methyl phenyl sulfoxide (PMSO) was used as a probe because PMSO could be oxidized by Fe(IV) and generate methyl phenyl sulfone ($PMSO_2$) via a two-electron process accompanied with an oxygen atom transfer from $Fe^{IV}=O^{2+}$ to PMSO (Zhu *et al.* 2020). Namely, $Fe^{IV}=O^{2+}$ reacts with PMSO and would cause the concentration decrease of PMSO, and equivalent $PMSO_2$ would be generated simultaneously. As can be seen in Figure 4(a), about 3.8% of PMSO was oxidized by PMS solution and equivalent $PMSO_2$ was generated. In the Fe^{3+}/GA/PMS system, 87.6% of PMSO was degraded within 10 min, and 44.2% of $PMSO_2$ was generated. The result demonstrated that $PMSO_2$ was significantly generated with the degradation of PMSO simultaneously, indicating the existence of $Fe^{IV}=O^{2+}$ species. If the ferryl species is the unique ROS in the system, the PMSO degraded (mole) would be the same as $PMSO_2$ generated (mole). In the Fe^{3+}/GA/PMS system, 43.8 μmol of PMSO was degraded with 22.1 μmol of generated $PMSO_2$. The $PMSO_2$ yield rate could be calculated as 50.4%. This observation demonstrated that part of PMSO was directly degraded by radicals in the system, rendering the low $PMSO_2$ yield. To prove the existence of $Fe^{IV}=O^{2+}$, benzoic acid (BA) was used as scavenger because Fe(IV) species are of high reactivity with

Downloaded from http://iwaponline.com/ws/article-pdf/22/5/4852/1076437/ws022054852.pdf
by guest

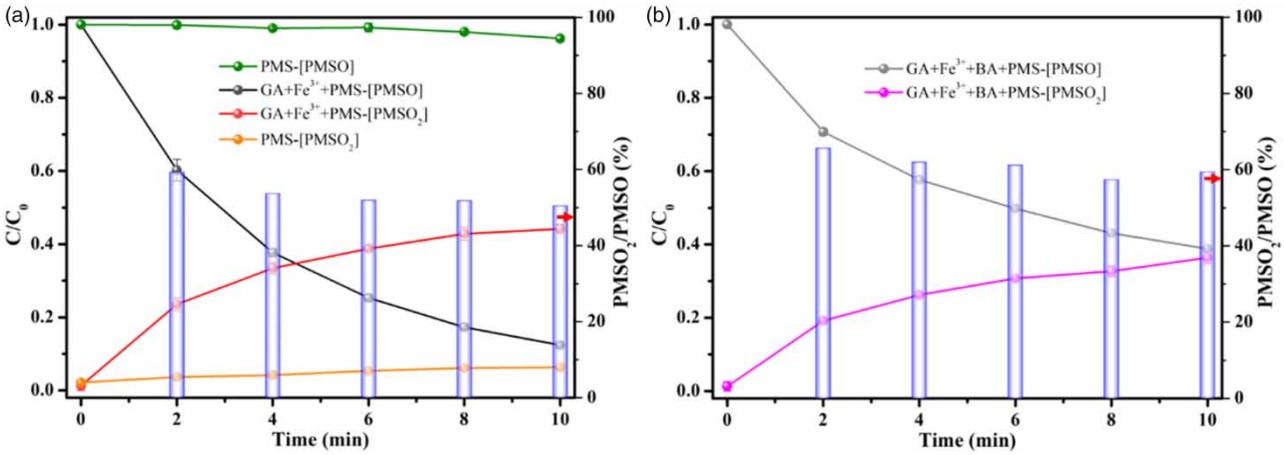

Figure 4 | Ferryl species investigation (a) Fe^{3+}/GA/PMS system and (b) Fe^{3+}/GA/PMS/BA system ([Fe^{3+}] = 100 μM, [GA] = 100 μM, [PMS] = 1 mM, [PMSO] = 500 μM, [BA] = 50 μM, [pH_0] = 5.0 ± 0.1, [Temperature] = 25 ± 0.2 °C).

PMSO but inert to react with BA (Dong *et al.* 2021). The results showed that the existence of BA significantly inhibited the degradation of PMSO but negligibly affected the generation of $PMSO_2$. The $PMSO_2$ yield rate increased to 59.41%. Therefore, it can be seen that both Fe(IV), $SO_4^{\cdot-}$, and $HO^{\cdot}$ was responsible for the organic degradation.

3.4. Catalytic mechanism

The nature of catalytic activation of PMS is basically an intentional cleavage of O-O bond and S-O bond in structure (HO-O-SO_3^-). For the O-O bond cleavage, free radicals like $SO_4^{\cdot-}$ and $HO^{\cdot}$ would be produced (Duan *et al.* 2016). On the other hand, prolonged S-O bond always primarily respond to the generation of HOO* and O_2^- species, which facilitated the oxidation performance obliquely (Nie *et al.* 2020). Considering the results of ROS identification, both O-O bond and S-O bond cleavage were all involved. The O-O bond cleavage of PMS usually primarily occurred when PMS was activated by external energy or electrons. Thus, it can be concluded that the extra electrons were released by Fe^{3+}-GA complex, and transferred to PMS. Therefore, the self-oxidation of gallic acid should be evaluated.

In-situ ATR-FTIR analysis was used to investigate the coordination site between GA and Fe^{3+}. As shown in Figure 5(c), two peaks located at 3428 and 1650 cm^{-1} could be observed in GA, corresponding to the phenolic hydroxyl groups and carboxylic groups, respectively (Jiang *et al.* 2021). After GA coordinated with Fe^{3+}, the vibration of -OH and -COOH were all blue-shifted. Therein -OH groups exhibited stronger blue shift from 3428 and 3305 cm^{-1} than -COOH (from 1650 to 1639 cm^{-1}). This observation demonstrated that Fe^{3+} mainly coordinated with GA at the phenolic hydroxyl sites, which is similar to existing literature (Nguyen *et al.* 2015). In addition, the existence of PMS did not influence the vibration of the Fe^{3+}/GA complex.

Against this background, density functional theory (DFT) calculation was used to analyze the electron structure of GA and Fe^{3+}/GA complex. Fukui function was always used to investigate the reaction sites in organic molecules. Therefore, the Fukui index of GA was firstly calculated (Duan *et al.* 2021). Figure 5(a-1) exhibits that both C atom in ring and O atom in hydroxyl and carboxylic groups readily react with electrophilic attack, and clearly manifested the self-oxidation sites of GA molecule. Figure 5(a-2) shows that the coordination site in bidentate Fe^{3+}-GA complex possessed stronger tendency than GA to react with electrophilic attack. Namely, the sites that are sensitive to electrophilic attack tended to release electrons, and therefore Fe^{3+} coordinated with GA would be reduced. This tendency could be attributed to the π-electron delocalization in GA molecule. Localization orbital locator (LOL) analysis shown in Figure 5(b-1) exhibited the delocalization behavior of π-electron in GA. When GA is coordinated with Fe^{3+} (Figure 5(b-2)), the electronic structure of GA is totally redistributed. The delocalizable electrons density in the ring tended to decrease, and then concentrate on the coordination (Fe) site, further proving the possibility of Fe^{3+} reduction into Fe^{2+} during the oxidation of GA.

The self-oxidation of GA is further evaluated through electrochemical analysis. Figure 5(d) exhibited the pH-dependent cyclic voltametric (CV) behavior of GA. Two anodic CV peaks could be observed with the non-existence of counter-peaks, indicating the self-oxidation of hydroxyl groups in GA with simultaneous electron release. The non-detectable counter-peaks demonstrated that the oxidation of GA is irreversible. As discussed before, solution pH significantly influenced its

Downloaded from http://iwaponline.com/ws/article-pdf/22/5/4852/1076437/ws022054852.pdf
by guest

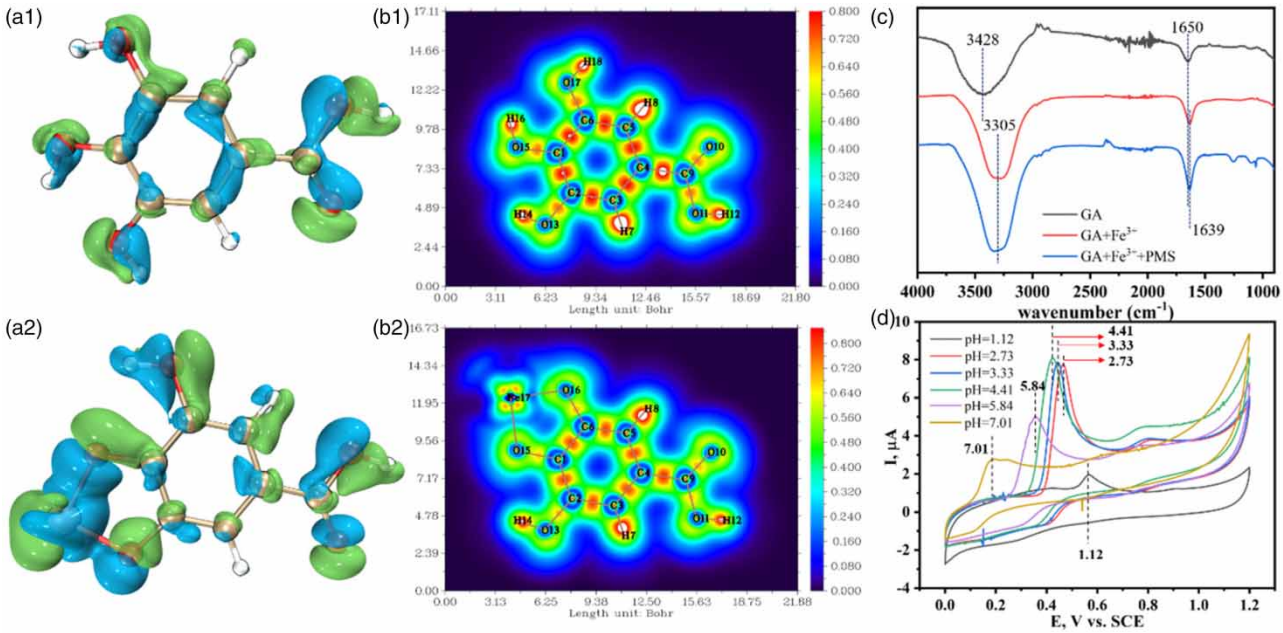

Figure 5 | (a-1) Fukui function of GA, (a-2) Fukui function of bidentate Fe^{3+}-GA complex, (b-1) LOL analysis of GA, (b-2) LOL analysis of bidentate Fe^{3+}-GA complex, (c) ATR-FTIR analysis of GA, Fe^{3+}/GA, and Fe^{3+}/GA/PMS system, and (d) cyclic voltametric analysis of GA at different solution pH which buffered by phosphate solution ([Fe^{3+}] = 100 μM, [GA] = 100 μM, [phosphate buffer] = 100 mM, scan rate: 50 mV/s).

PMS activation. Therefore, CV analysis under different solution pH was further conducted. As shown in Figure 5(d), the two peaks could be observed in all tests when pH was lower than 7.01. The primary potential peaks shifted to the low potential area with the increase of pH, demonstrating that the self-oxidation of GA is related to the activity/concentration of H^+ in solution. In brief, higher solution pH would facilitate the deprotonation and electron release of GA. The Fe^{3+} in the complex would be therefore reduced to Fe^{2+} by the released electrons during the oxidation of GA, rendering continuously activated PMS by the regenerated Fe^{2+}. Therefore, the CV curve of Fe^{3+}/GA complex was also evaluated (Figure S2). However, the counter-wave still cannot be observed clearly, possibly indicating that the product generated by GA oxidation blocked the surface of the electrode. As mentioned above, the Fe^{3+}/GA/PMS exhibited more overwhelming BPA degradation than Fe^{3+}/PMS. It also should be restated that GA/PMS exhibited negligible BPA degradation performance. Therefore, the Fe^{3+}/Fe^{2+} cycling in the process should be confirmed, and higher solution pH would cause elevated self-oxidation of GA. To prove this conclusion, 1,10-Phenanthroline (*phen*) was added into the Fe^{3+}-GA system as phen could effectively coordinate with Fe^{2+} ions. The complex formed by Fe^{2+} and *phen* is red color which can be measured via a UV-vis spectrometer at 510 nm. The result showed that the color of the Fe^{3+}/GA solution suddenly turned red once *phen* was added (inset in Figure 6(a)), and the concentration of Fe^{2+} was almost the same with Fe^{3+}. Therefore, the Fe^{3+}/Fe^{2+} cycle triggered by GA was confirmed. Considering the CV behavior of GA, it can be proposed that Fe^{2+} was generated through the following chain reactions:

$$Fe^{3+} - GA \rightarrow Fe^{3+} - GA^{\cdot} + e^{-} \rightarrow Fe^{2+} - GA^{\cdot+} \quad (1)$$

$$Fe^{2+} - GA^{\cdot+} + HOOSO_3^- \rightarrow Fe^{3+} - GA^{\cdot} + SO_4^{\cdot-}/HO^{\cdot} + H_2O/SO_4^{2-} \quad (2)$$

$$Fe^{3+} - GA^{\cdot} \rightarrow Fe^{3+} - GA^{+} + e^{-} \rightarrow Fe^{2+} - GA^{+} \quad (3)$$

$$Fe^{2+} - GA^{+} + HOOSO_3^- \rightarrow Fe^{3+} - GA_O + SO_4^{\cdot-}/HO^{\cdot} + H_2O/SO_4^{2-} \quad (4)$$

$$HOOSO_3^- + Fe^{3+} \rightarrow SO_5^{\cdot-} + Fe^{2+} + H_2O \quad (5)$$

$$2SO_5^{\cdot-} \rightarrow 2SO_4^{\cdot-} + O_2 \quad (6)$$

$$Fe^{2+} - GA^{\cdot+} + O_2 + 2H^{+} \rightarrow Fe^{3+} - GA_O + H_2O_2 \quad (7)$$

Downloaded from http://iwaponline.com/ws/article-pdf/22/5/4852/1076437/ws022054852.pdf
by guest

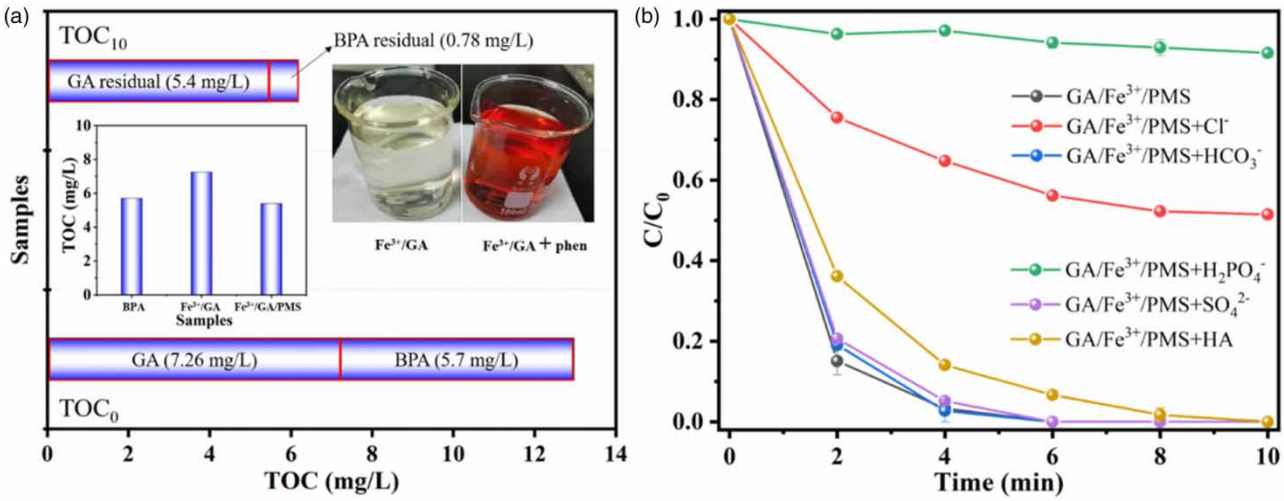

Figure 6 | (a) mineralization (inset: the picture of Fe^{3+}-GA complex before and after addition of *phen*) and (b) effect of coexisting chemicals ([BPA] = 40 μM, [Fe^{3+}] = 100 μM, [GA] = 100 μM, [PMS] = 1 mM, [Cl^-] = [HCO_3^-] = [HPO_4^-] = [SO_4^{2-}] = 500 μM, [HA] = 20 mg/L, [pH_0] = 5.0 ± 0.1, [Temperature] = 25 ± 0.2 °C).

Fe^{3+} was firstly coordinated with GA in solution, rendering the complex of Fe^{3+}-GA. The decay (self-oxidation) of GA would release electrons and form $GA^{\bullet+}$ radicals, which could reduce the metal center from Fe^{3+} into Fe^{2+} (Equation (1)). The Fe^{2+} centered complex would then coordinate with PMS, and the PMS would be decomposed, generating $SO_4^{\bullet-}$ or $HO^{\bullet}$ radicals and Fe^{3+}-$GA^{\bullet}$ (Equation (2)). Further decay of the complex would reduce the metal center into Fe^{2+} and then activate PMS to produce $SO_4^{\bullet-}$/$HO^{\bullet}$ (Equations (3) and (4)). The coordinated GA was finally transformed into GA-quinone compound. On the other hand, the coordination of Fe^{2+}-GA species and PMS would cause heterolytic cleavage of PMS, rendering the formation of GA-$Fe^{4+}=O^{2+}$. GA-$Fe^{4+}=O^{2+}$ with strong oxidation capacity would oxidize BPA and form Fe^{3+}-GA species, which can be proven by the PMSO-$PMSO_2$ probe experiment. In addition, dioxygen released from the decay of PMS would be reduced by Fe^{3+}/GA complex and generate O_2^- and H_2O_2, which explained the results obtained from EPR analysis (Equations (5)–(7)).

3.5. Mineralization and the effect of water matrices

The mineralization performance was evaluated by TOC analysis. As shown in Figure 6(a), TOC supplied by BPA in influent was 5.7 mg/L, where GA accounted for 7.26 mg/L. After Fe^{3+}/GA reacted with PMS without the existence of BPA, TOC decreased to 5.4 mg/L. On the other hand, TOC of the Fe^{3+}/GA/PMS/BPA system after 10 min (TOC_{10}) was measured as 6.18 mg/L. This result demonstrated that more than 86.4% of BPA was not only degraded, but also mineralized, indicating the significant BPA mineralization performance of the Fe^{3+}/GA/PMS system. More importantly, although the added GA attenuated from 7.26 to 5.4 mg/L after facilitating the Fe^{3+}/H_2O_2 process for BPA degradation, the residual GA still should be noted as secondary pollution caused by the residual GA is not expected. For the removal of residual GA, coagulation was employed by adding poly-aluminum chloride (PAC, 5 mg/L). The results show that TOC contributed by the residual GA was almost totally removed. Therefore, the risk of possible secondary pollution by the residual GA could be well solved.

Various coexisting anions and organic substances widely coexist in natural water bodies. Therefore, the effect of coexisting anions was finally evaluated. The results showed that the effect of HCO_3^- and SO_4^{2-} on the BPA degradation are negligible (Figure 6(b)) (Jiang *et al.* 2017). However, the existence of Cl^- exhibited significant inhibition, which is shown in Figure 6(b). It has been reported that Cl^- would react with $SO_4^{\bullet-}$/$HO^{\bullet}$ and form $Cl^{\bullet}$ with low redox potential, rendering the decreased BPA degradation performance. This phenomenon is the same as previous studies (Liu *et al.* 2016; Qiu *et al.* 2019).

The effect of phosphate (PO_4^{3-}) was also evaluated. As shown in Figure 6(a), the existence of PO_4^{3-} exhibited significant inhibition as BPA degradation by Fe^{3+}/GA/PMS was totally terminated. The plausible reason responsible to this phenomenon is that phosphate readily reacts and precipitates with Fe^{3+}/Fe^{2+} ions. The precipitation of Fe^{3+} and PO_4^{3-} would totally deactivate the catalytic performance of Fe species, which is similar to the hydrolysis of Fe^{3+} to form $Fe(OH)_3$.

Downloaded from http://iwaponline.com/ws/article-pdf/22/5/4852/1076437/ws022054852.pdf
by guest

Finally, the effect of coexisting organic substances was simulated by using humic acid (HA) as the representative background. It can be seen that the existence of HA in the Fe^{3+}/GA/PMS system significantly inhibited the BPA degradation (Yang *et al.* 2021b). However, the BPA still can be completely degraded within 10 min, demonstrating the considerable oxidation performance.

4. CONCLUSION

In this study, gallic acid (GA) was used as a promoter in the Fe^{3+}/PMS system for efficient bisphenol A (BPA) degradation. The results show that BPA could be effectively degraded by the Fe^{3+}/PMS process with the addition of GA. EPR and scavenging studies manifested that $SO_4^{\bullet-}$, $HO^{\bullet}$, O_2^{-}, and $^1O_2$ were generated in the process, where $SO_4^{\bullet-}$, $HO^{\bullet}$, and ferryl species played the dominant role for BPA degradation. The Fe^{3+}/GA/PMS process exhibited the best oxidation efficiency at neutral and slightly alkaline conditions. Both strong acid and alkaline conditions negatively affected the BPA degradation. In addition, the molar ratio of Fe^{3+}:GA = 1:1 was found to be the most effective condition, lower molar ratio of Fe^{3+}: GA would inhibit the BPA degradation. The coordination between Fe^{3+} and GA could effectively prevent the hydrolysis of Fe^{3+}, and maintain the catalytic activity of Fe^{3+}. Electrochemical analysis proved that the self-oxidation of GA would release electrons and reducing Fe^{3+} metal center into Fe^{2+}, rendering a continuously activated Fenton-like reaction. Finally, the coexistence of phosphate in solution could significantly inhibit oxidation of the Fe^{3+}/GA/PMS process, which should be noted. The results of this study shed light on preventing Fe^{3+} hydrolysis and facilitating Fe^{3+}/Fe^{2+} cycling simultaneously in Fenton-like reaction and more related studies are needed to evaluate its potential in actual applications.

ACKNOWLEDGEMENT

This research was supported by the National Natural Science Foundation of China (Grant No. 51508451) and the new style think tank of Shaanxi Universities (20JT041).

DECLARATIONS OF INTEREST

None.

DATA AVAILABILITY STATEMENT

All relevant data are included in the paper or its Supplementary Information.

REFERENCES

Chen, X., Vione, D., Borch, T., Wang, J. & Gao, Y. 2021 Nano-MoO_2 activates peroxymonosulfate for the degradation of PAH derivatives. *Water Research* **192**, 116834.

Dong, H., Xu, Q., Lian, L., Li, Y., Wang, S., Li, C. & Guan, X. 2021 Degradation of organic contaminants in the Fe(II)/peroxymonosulfate process under acidic conditions: the overlooked rapid oxidation stage. *Environmental Science & Technology* **55**, 15390–15399.

Duan, X., Sun, H., Ao, Z., Zhou, L., Wang, G. & Wang, S. 2016 Unveiling the active sites of graphene-catalyzed peroxymonosulfate activation. *Carbon* **107**, 371–378.

Duan, J., Chen, L., Ji, H., Li, P., Li, F. & Liu, W. 2021 Activation of peracetic acid by metal-organic frameworks (ZIF-67) for efficient degradation of sulfachloropyridazine. *Chinese Chemical Letters*. In press, https://doi.org/10.1016/j.cclet.2021.11.096.

Gao, Y., Han, Y., Liu, B., Gou, J., Feng, D. & Cheng, X. 2021 $CoFe_2O_4$ nanoparticles anchored on waste eggshell for catalytic oxidation of florfenicol via activating peroxymonosulfate. *Chinese Chemical Letters*. In press, https://doi.org/10.1016/j.cclet.2021.11.072.

Gaussian 16, Revision C.01, Frisch, M. J., Trucks, G. W., Schlegel, H. B., Scuseria, G. E., Robb, M. A., Cheeseman, J. R., Scalmani, G., Barone, V., Petersson, G. A., Nakatsuji, H., Li, X., Caricato, M., Marenich, A. V., Bloino, J., Janesko, B. G., Gomperts, R., Mennucci, B., Hratchian, H. P., Ortiz, J. V., Izmaylov, A. F., Sonnenberg, J. L., Williams-Young, D., Ding, F., Lipparini, F., Egidi, F., Goings, J., Peng, B., Petrone, A., Henderson, T., Ranasinghe, D., Zakrzewski, V. G., Gao, J., Rega, N., Zheng, G., Liang, W., Hada, M., Ehara, M., Toyota, K., Fukuda, R., Hasegawa, J., Ishida, M., Nakajima, T., Honda, Y., Kitao, O., Nakai, H., Vreven, T., Throssell, K., Montgomery Jr., J. A., Peralta, J. E., Ogliaro, F., Bearpark, M. J., Heyd, J. J., Brothers, E. N., Kudin, K. N., Staroverov, V. N., Keith, T. A., Kobayashi, R., Normand, J., Raghavachari, K., Rendell, A. P., Burant, J. C., Iyengar, S. S., Tomasi, J., Cossi, M., Millam, J. M., Klene, M., Adamo, C., Cammi, R., Ochterski, J. W., Martin, R. L., Morokuma, K., Farkas, O., Foresman, J. B. & Fox, D. J. 2019. Gaussian, Inc., Wallingford, CT.

Guan, Y.-H., Ma, J., Li, X.-C., Fang, J.-Y. & Chen, L.-W. 2011 Influence of pH on the formation of sulfate and hydroxyl radicals in the UV/Peroxymonosulfate system. *Environmental Science & Technology* **45**, 9308–9314.

Downloaded from http://iwaponline.com/ws/article-pdf/22/5/4852/1076437/ws022054852.pdf
by guest

Huang, B., Xiong, Z., Zhou, P., Zhang, H., Pan, Z., Yao, G. & Lai, B. 2022 Ultrafast degradation of contaminants in a trace cobalt(II) activated peroxymonosulfate process triggered through borate: indispensable role of intermediate complex. *Journal of Hazardous Materials* **424**, 127641.

Jiang, M., Lu, J., Ji, Y. & Kong, D. 2017 Bicarbonate-activated persulfate oxidation of acetaminophen. *Water Research* **116**, 324–331.

Jiang, J., Zhang, S., Longhurst, P., Yang, W. & Zheng, S. 2021 Molecular structure characterization of bituminous coal in Northern China via XRD, Raman and FTIR spectroscopy. *Spectrochimica Acta Part A: Molecular and Biomolecular Spectroscopy* **255**, 119724.

King, C. V. 1928 Silver ion catalysis of persulfate oxidations. III. The oxidation of ammonium ion1. *Journal of the American Chemical Society* **50**, 2080–2088.

Li, J., Fang, J., Gao, L., Zhang, J., Ruan, X., Xu, A. & Li, X. 2017 Graphitic carbon nitride induced activity enhancement of OMS-2 catalyst for pollutants degradation with peroxymonosulfate. *Applied Surface Science* **402**, 352–359.

Li, D., Zheng, T., Yu, J., He, H., Shi, W. & Ma, J. 2022 Enhancement of the electro-Fenton degradation of organic contaminant by accelerating Fe^{3+}/Fe^{2+} cycle using hydroxylamine. *Journal of Industrial and Engineering Chemistry* **105**, 405–413.

Liu, Y., Guo, H., Zhang, Y., Tang, W., Cheng, X. & Liu, H. 2016 Activation of peroxymonosulfate by $BiVO_4$ under visible light for degradation of Rhodamine B. *Chemical Physics Letters* **653**, 101–107.

Lu, T. & Chen, F. 2012 Multiwfn: a multifunctional wavefunction analyzer. *Journal of Computational Chemistry* **33**, 580–592.

Meng, F., Zhang, S., Zeng, Y., Zhang, M., Zou, H., Zhong, Q. & Li, Y. 2021 Promotional effect of surface fluorine on TiO_2: catalytic conversion of O_3 and $H2O_2$ into ·OH and $·O^{2-}$ radicals for high-efficiency NO oxidation. *Chemical Engineering Journal* **424**, 130358.

Miao, J., Geng, W., Alvarez, P. J. J. & Long, M. 2020 2D N-doped porous carbon derived from polydopamine-coated graphitic carbon nitride for efficient nonradical activation of peroxymonosulfate. *Environmental Science & Technology* **54**, 8473–8481.

Milh, H., Cabooter, D. & Dewil, R. 2021 Role of process parameters in the degradation of sulfamethoxazole by heat-activated peroxymonosulfate oxidation: radical identification and elucidation of the degradation mechanism. *Chemical Engineering Journal* **422**, 130457.

Nguyen, D. M. T., Zhang, Z. & Doherty, W. O. S. 2015 Degradation of hydroxycinnamic acid mixtures in aqueous sucrose solutions by the Fenton process. *Journal of Agricultural and Food Chemistry* **63**, 1582–1592.

Nie, C., Dai, Z., Liu, W., Duan, X., Wang, C., Lai, B., Ao, Z., Wang, S. & An, T. 2020 Criteria of active sites in nonradical persulfate activation process from integrated experimental and theoretical investigations: boron–nitrogen-co-doped nanocarbon-mediated peroxydisulfate activation as an example. *Environmental Science: Nano* **7**, 1899–1911.

Ouyang, D., Chen, Y., Chen, R., Zhang, W., Yan, J., Gu, M., Li, J., Zhang, H. & Chen, M. 2022 Degradation of 1,4-dioxane by biochar activating peroxymonosulfate under continuous flow conditions. *Science of The Total Environment* **809**, 151929.

Qiu, X., Yang, S., Dzakpasu, M., Li, X., Ding, D., Jin, P., Chen, R., Zhang, Q. & Wang, X. C. 2019 Attenuation of BPA degradation by SO^{4-} in a system of peroxymonosulfate coupled with Mn/Fe MOF-templated catalysts and its synergism with Cl^- and bicarbonate. *Chemical Engineering Journal* **372**, 605–615.

Qiu, X., Ding, D., Yang, S., Wang, G., Chen, R., Dzakpasu, M., Jin, P. & Wang, X. C. 2021 Solid-state synthesis of cobalt ferrite fitted with γ-Fe_2O_3-containing nanocage for peroxymonosulfate activation and cobalt leaching control. *Chemical Engineering Journal* **405**, 126994.

Ristić, M., Musić, S. & Godec, M. 2006 Properties of γ-FeOOH, α-FeOOH and α-Fe_2O_3 particles precipitated by hydrolysis of Fe^{3+} ions in perchlorate containing aqueous solutions. *Journal of Alloys and Compounds* **417**, 292–299.

Shen, J., Zhao, H., Cao, H., Zhang, Y. & Chen, Y. 2014 Removal of total cyanide in coking wastewater during a coagulation process: significance of organic polymers. *Journal of Environmental Sciences* **26**, 231–239.

Sirés, I., Centellas, F., Garrido, J. A., Rodríguez, R. M., Arias, C., Cabot, P.-L. & Brillas, E. 2007 Mineralization of clofibric acid by electrochemical advanced oxidation processes using a boron-doped diamond anode and Fe^{2+} and UVA light as catalysts. *Applied Catalysis B: Environmental* **72**, 373–381.

Song, X., Tian, J., Shi, W., Cui, F. & Yuan, Y. 2020 Significant acceleration of Fe^{2+}/peroxydisulfate oxidation towards sulfisoxazole by addition of MoS_2. *Environmental Research* **188**, 109692.

Wang, S., Xu, W., Wu, J., Gong, Q. & Xie, P. 2020a Improved sulfamethoxazole degradation by the addition of MoS_2 into the Fe^{2+}/peroxymonosulfate process. *Separation and Purification Technology* **235**, 116170.

Wang, G., Qin, J., Feng, Y., Feng, B., Yang, S., Wang, Z., Zhao, Y. & Wei, J. 2020b Sol–gel synthesis of spherical mesoporous high-entropy oxides. *ACS Applied Materials & Interfaces* **12**, 45155–45164.

Wang, Z., Qiu, W., Pang, S., Gao, Y., Zhou, Y., Cao, Y. & Jiang, J. 2020c Relative contribution of ferryl ion species (Fe(IV)) and sulfate radical formed in nanoscale zero valent iron activated peroxydisulfate and peroxymonosulfate processes. *Water Research* **172**, 115504.

Wang, T., Zhou, J., Wang, W., Zhu, Y. & Niu, J. 2021a Ag-single atoms modified S1.66-N1.91/TiO_2-x for photocatalytic activation of peroxymonosulfate for bisphenol A degradation. *Chinese Chemical Letters*. In press, https://doi.org/10.1016/j.cclet.2021.08.085.

Wang, T., de Vos, W. M. & de Grooth, J. 2021b $CoFe_2O_4$-peroxymonosulfate based catalytic UF and NF polymeric membranes for naproxen removal: the role of residence time. *Journal of Membrane Science* **646**, 120209.

Wang, X., Cai, W., Ye, D., Zhu, Y., Cui, M., Xi, J., Liu, J. & Xing, W. 2021c Bio-based polyphenol tannic acid as universal linker between metal oxide nanoparticles and thermoplastic polyurethane to enhance flame retardancy and mechanical properties. *Composites Part B: Engineering* **224**, 109206.

Wang, Y., Fang, L., Wang, Z. & Yang, Q. 2021d Peroxymonosulfate activation by graphitic carbon nitride co-doped with manganese, cobalt, and oxygen for degradation of trichloroethylene: effect of oxygen precursors, kinetics, and mechanism. *Separation and Purification Technology* **278**, 119580.

Downloaded from http://iwaponline.com/ws/article-pdf/22/5/4852/1076437/ws022054852.pdf
by guest

Wei, J., Liang, Y., Hu, Y., Kong, B., Zhang, J., Gu, Q., Tong, Y., Wang, X., Jiang, S. P. & Wang, H. 2016 Hydrothermal synthesis of metal–polyphenol coordination crystals and their derived metal/N-doped carbon composites for oxygen electrocatalysis. *Angewandte Chemie International Edition* **55**, 12470–12474.

Yang, S., Xu, S., Tong, J., Ding, D., Wang, G., Chen, R., Jin, P. & Wang, X. C. 2021a Overlooked role of nitrogen dopant in carbon catalysts for peroxymonosulfate activation: intrinsic defects or extrinsic defects? *Applied Catalysis B: Environmental* **295**, 120291.

Yang, H., Luo, B., Lei, S., Wang, Y., Sun, J., Zhou, Z., Zhang, Y. & Xia, S. 2021b Enhanced humic acid degradation by Fe_3O_4/ultrasound-activated peroxymonosulfate: synergy index, non-radical effect and mechanism. *Separation and Purification Technology* **264**, 118466.

Zhang, Y., Klamerth, N. & Gamal El-Din, M. 2016 Degradation of a model naphthenic acid by nitrilotriacetic acid – modified Fenton process. *Chemical Engineering Journal* **292**, 340–347.

Zhou, T., Li, Y., Wong, F.-S. & Lu, X. 2008 Enhanced degradation of 2,4-dichlorophenol by ultrasound in a new Fenton like system (Fe/EDTA) at ambient circumstance. *Ultrasonics Sonochemistry* **15**, 782–790.

Zhu, J., Yu, F., Meng, J., Shao, B., Dong, H., Chu, W., Cao, T., Wei, G., Wang, H. & Guan, X. 2020 Overlooked role of Fe(IV) and Fe(V) in organic contaminant oxidation by Fe(VI). *Environmental Science & Technology* **54**, 9702–9710.

First received 7 January 2022; accepted in revised form 13 March 2022. Available online 31 March 2022

Downloaded from http://iwaponline.com/ws/article-pdf/22/5/4852/1076437/ws022054852.pdf
by guest